International Journal of Pharmaceutics 420 (2011) 385–394

Contents lists available at SciVerse ScienceDirect

International Journal of Pharmaceutics

journal homepage: www.elsevier.com/locate/ijpharm

Pharmaceutical Nanotechnology

PEGylated poly(trimethylene carbonate) nanoparticles loaded with paclitaxel for the treatment of advanced glioma: In vitro and in vivo evaluation

Xinyi Jiang[a,b], Hongliang Xin[a,b], Xianyi Sha[a,b], Jijin Gu[a,b], Ye Jiang[a,b], Kitki Law[a,b,c], Yanzuo Chen[a,b], Liangcen Chen[a,b], Xiao Wang[a,b], Xiaoling Fang[a,b,*]

[a] Department of Pharmaceutics, School of Pharmacy, Fudan University, 826 Zhangheng Rd., Shanghai 201203, People's Republic of China
[b] Key Laboratory of Smart Drug Delivery (Fudan University), Ministry of Education & PLA, 826 Zhangheng Rd., Shanghai 201203, People's Republic of China
[c] Department of Pharmacy, Huashan Hospital, Fudan University, Shanghai 200040, People's Republic of China

ARTICLE INFO

Article history:
Received 7 July 2011
Received in revised form 5 August 2011
Accepted 31 August 2011
Available online 6 September 2011

Keywords:
MPEG–PTMC
Paclitaxel
Nanoparticle
Glioblastoma multiforme
Drug delivery

ABSTRACT

The aim of this study was to investigate the antitumor effect of paclitaxel (PTX)-loaded poly(ethylene glycol)–poly(trimethylene carbonate) (MPEG–PTMC) nanoparticles (NP) against gioblastoma multiforme (GMB). PTX-loaded NP (NP/PTX) were prepared with synthesized MPEG–PTMC by the emulsion/solvent evaporation technique. In vitro physiochemical characterization of those NP/PTX showed satisfactory encapsulation efficiency and loading capacity and size distribution. Cytotoxicity assay revealed that encapsulation in nanoparticles did not compromise the antitumor efficacy of PTX against U87MG cells. Pharmacokinetic study in rats demonstrated that the polymer micellar nanoparticles significantly enhanced the bioavailability of PTX than Taxol. In intracranial xenograft tumor-bearing mice, the accumulation of nanoparticles in tumor tissues increased distinctly after 12 h post i.v. More importantly, in vivo anti-tumor effect exhibited the median survival time of NP/PTX treated mice (27 days) was significantly longer than those of mice treated with Taxol (24 days), physiological saline (21 days) and blank MPEG–PTMC NP (21 days). Therefore, our results suggested that PTX-loaded MPEG–PTMC nanoparticles significantly enhanced the anti-glioblastoma activity of PTX and may be a potential vehicle in the treatment of high-grade glioma.

1. Introduction

According to the WHO classification of cerebral glioma, glioma is divided into four grades: I, II, III, and IV glioma (Kleihues et al., 1993; Louis et al., 2007; Zülch, 1980). And the low-grade tumors usually evolved into a high-grade glioblastoma multiforme (GBM). GBM are highly angiogenic tumors and, consequently, these tumors harbor new and leaky blood vessels and lack of the effective lymphatic drainage system (Law et al., 2004; Lupo et al., 2005; Plate and Risau, 1995). It could cause edema, which is the consequence of a local disruption of the BBB by impaired capillary endothelial tight junctions (Groothuis et al., 1991; Leggett et al., 1998; Lu et al., 2008; Sameshima et al., 2000; Schneider et al., 2004; Wolburg et al., 2003). According to the pathological conditions of glioma in different grades, the different strategies should be taken to the design of the drug delivery system targeting glioma. When the glioma is still low-grade, the BBB is intact and the drug delivery system should be able to cross the BBB and further target to glioma (Huang et al., 2011). However, when it develops to advanced-grade, drug delivery system can accumulate in the glioma by the enhanced permeability and retention (EPR) effect.

PTX, a promising anticancer drug isolated from the bark of *Taxus brevifolia*, has been proven effective in the treatment of gliomas (Nikanjam et al., 2007; Regina et al., 2008). Despite the successful properties exhibited by this drug for several cancers, its utility in the clinic is hampered by severe limitations such as poor aqueous solubility and serious side effects due to its non-selective distribution in vivo. Clinically, the current formulation for PTX is made with Cremophor EL (polyethoxylated castor oil and ethanol, 50:50. Taxol), which should be diluted in saline prior to intravenous administration. Unfortunately, this formulation caused severe adverse allergic reactions due to histamine release and hypersensitivity reactions (Musacchio et al., 2008). Various drug delivery systems (DDS) have been developed to overcome these deficiencies, including micelles, nanoparticles and liposomes (Danhier et al., 2009; Xin et al., 2010; Zhan et al., 2010; Zhao et al., 2009). Among these DDS being applied to PTX, self-assembled nanoparticles, composed of polymer amphiphiles, have been considered to be effective carriers because they can stay unrecognized during blood circulation, reduce the adverse reactions and increase the therapeutic efficacy.

* Corresponding author at: Department of Pharmaceutics, School of Pharmacy, Fudan University, 826 Zhangheng Rd., Shanghai 201203, People's Republic of China. Tel.: +86 21 51980071; fax: +86 21 51980072.
E-mail address: xlfang@shmu.edu.cn (X. Fang).

0378-5173/$ – see front matter © 2011 Elsevier B.V. All rights reserved.
doi:10.1016/j.ijpharm.2011.08.052

Poly(trimethylene carbonate) (PTMC), a biodegradable polyester, has attracted much research interest due to their tunable biodegradability and biocompatibility (Rokicki, 2000; Zhang et al., 2006c). PTMC homopolymer and its block copolymer were stable in water, but could be degraded in vivo or in lipase solutions by an enzymatic surface erosion process without the formation of acidic compounds (Han et al., 2009; Pego et al., 2003; Rokicki, 2000; Watanabe et al., 2007; Zhang et al., 2006c). Although PTMC with high molecular weight is amorphous, PTMC with a relatively low molecular weight is semi-crystalline and has a melting temperature close to body temperature (Zhu et al., 1991). These unique properties render PTMC homo- and copolymers potential candidates for biomedical application such as controlled drug delivery. PEG as water soluble, biocompatible, non-toxic and nonimmunogenic material, could not only enhance biocompatibility but also favorably affect pharmacokinetics and tissue distribution (Mao et al., 2005; Veronese, 2001). In present work, low molecular amphiphilic MPEG–PTMC containing high percentage of PEG segment was synthesized by ring opening polymerization. In an aqueous medium, these copolymers self-assemble to form core–shell type nanoparticles. The hydrophobic core may serve as a nanoreservoir for loading hydrophobic drugs and the PEG shell could endow the nanoparticles with a lower level of the reticuloendothelial system (RES) uptake and hence a prolonged circulation half-life.

In this study, we aimed to investigate the delivery efficiency of those copolymer-based nanocarriers for insoluble anticancer drugs, such as PTX, in vitro and in vivo. To achieve this aim, PTX-loaded MPEG–PTMC nanoparticles by the emulsion/solvent evaporation technique. The physicochemical characteristics, in vitro drug release, in vitro cell uptake characteristics and in vivo harmacokinetics in rats were investigated, respectively. And also, biodistribution and intracranial tumor accumulation of fluorescein-labeled NP were evaluated by non-invasive and real-time NIR imaging systems. Furthermore, the in vitro antitumoral activity of NP/PTX against U87MG cells was assessed and in vivo antitumor pharmacological effect in intracranial tumor-bearing mice was evaluated.

2. Materials and methods

2.1. Materials, cells and animals

PTX was purchased from Xi'an San jiang Bio-Engineering Co. Ltd. (Xi'an, China). Taxol injection (Anzatax Injection Concentrate, 30 mg/5 ml) was produced by FH Faulding & Co. Ltd. trading as David Bull Lab (Melbourne, Australia). Cremophor EL was kindly supplied by BASF Ltd. (Shanghai, China). Methoxy poly(ethylene glycol) (MPEG-OH, Mn is 3.0 kDa) was obtained from JenKem technology Co. LTD (Beijing, China). Polymer grade 1,3-trimethylene carbonate, namely, 1,3-dioxan-2-one (TMC) was purchased from Adamas Corporation (Shanghai local agent, China). Stannous octate ($Sn(Oct)_2$, Aldrich) was distilled prior to use. 1,1′-Dioctadecyl-3,3,3′,3′-tetramethylindotricarbocyanine iodide (DiR) was purchased from Biotium (Invitrogen, USA). Coumarin 6, 3-(4,5-dimethyl-thiazol-2-yl)-2,5-diphenyl-tetrazolium bromide (MTT), was purchased from Sigma (St. Louis, MO, USA). Cellulose ester membranes (dialysis bag) with a molecular weight cut off value (MWCO) of 3500 (Greenbird Inc., Shanghai, China) were used in dialysis experiments. Deionized (DI) water was produced by a Millipore water purification system (Millipore Corporation, USA). All the other solvents were analytical or chromatographic grade.

U87MG cells were obtained from Shanghai Institute of Cell Biology. It was cultured in special Dulbecco's modified Eagle medium (DMEM, Gibco) supplemented with 10% fetal bovine serum (FBS, Gibco). Balb/c nude mice (4–5 weeks old) of 20 ± 2 g body weight and female Sprague–Dawley (SD) rats (200 ± 20 g) obtained from Experimental Animal Center of Fudan University. All animal protocols were approved by the Fudan University Institutional Animal Care and Use Committee. Mice were housed under standard humane conditions and had access to food and water ad libitum.

2.2. Preparation of MPEG–PTMC NP

MPEG–PTMC block copolymer was synthesized by the ring-opening polymerization with modified condition compared to the described previously (Zhang et al., 2006b). The details of the synthesis procedures as well as the NMR characterizations of the resulting copolymers can be found in the online version of this article as Supplementary Materials.

MPEG–PTMC nanoparticles were prepared through the emulsion/solvent evaporation technique according to the procedure described elsewhere (Zhang et al., 2004). Namely, 40 mg of MPEG–PTMC and different amounts of PTX in 1 ml dichloromethane added into 5 ml of 0.6% sodium cholate aqueous solution were slowly poured into the solution and then sonicated at 200 W on ice using a probe sonicator (Xin zhi Biotechnology Co. Ltd., China). The emulsion formed was added drop-wise on 30 ml of sodium cholate 0.3% under rapid magnetic stirring. After that, dichloromethane was evaporated by rotary vacuum at 40 °C. Nanoparticles were then centrifuged at 14,000 rpm at 4 °C for 45 min. After discarding the supernatant, nanoparticles were resuspended in 1 ml of physiological saline and kept at 4 °C for further use.

The preparation of fluorescein-labeled NP was the same as that of PTX-loaded nanoparticles, except that 16 μl coumarin 6 or 80 μl DiR (1 mg/ml stock solution in dichloromethane) was additionally added to dichloromethane containing copolymers before emulsification. Then, the free coumarin 6 or Dir was removed via CL-4B column (Hanhong Chemica Co. LTD, China).

2.3. Characterization of the nanoparticles

2.3.1. Particle size, surface charge and morphology

Particle mean size, size distribution and zeta potential of the NP were determined by dynamic light scattering (DLS) using a Zeta Potential/Particle Sizer Nicomp™ 380 ZLS (Pss. Nicomp™, Santa Barbara, USA). The analyses were performed with 5 mW He–Ne laser (632.8 nm) at a scattering angle of 90° at 25 °C. Each freshly prepared sample was diluted to the appropriate concentration using DI water to avoid multi-scattering phenomena and was placed into a quartz cuvette. The reported experimental result of each sample was expressed as a mean size ± SD for three separate experiments. The morphological examination of NP was observed by transmission electron microscope (TEM) (JEOL JMPEG-PTMC-1230, Japan) at an acceleration voltage of 200 kV after negative staining with phosphotungstic acid solution (2%, w/v).

2.3.2. Determination of PTX-loading content and encapsulation efficiency

To investigate the drug loading content (DLC%) and encapsulation efficiency (EE%), different amounts of PTX were co-dissolved with MPEG–PTMC in the preparation process of NP. The NP/PTX were diluted by acetonitrile and the concentration of PTX was measured via HPLC conducted by using a Shimadzu HPLC system equipped with a reversed-phase column (Gemini 5 μm C18, 200 mm × 4.6 mm, Phenomenex, California, USA), a LC-10ATVP pump, a SPD-10AVP UV detector (Shimadzu, Kyoto, Japan) and a HS2000 interface (Hangzhou Empire Science & Tech, Hangzhou, China) operated at 227 nm. The mobile phase was a mixture of acetonitrile and water (60:40, v/v), the flow rate was 1.0 ml/min,

and the detection wavelength was 227 nm. Sample solution was injected at a volume of 20 μl. The HPLC was calibrated with standard solutions of 0.5–50 μg/ml of PTX dissolved in acetonitrile (correlation coefficient of $R^2 = 0.9998$). The limit of quantification was 0.5 ng/ml. The coefficients of variation (CV) were all within 2.8%. The drug loading content (DLC%) and encapsulation efficiency (EE%) were obtained by the equations as follows:

$$\text{DLC}\% = \frac{\text{Amount of PTX in NP}}{\text{Amount of the feeding polymer and PTX}} \times 100\%$$

$$\text{EE}\% = \frac{\text{Amount of PTX in NP}}{\text{Amount of the feeding PTX}} \times 100\%$$

2.4. In vitro release profiles

The in vitro release behaviors of PTX from the NP/PTX were monitored in an aqueous medium containing 1 M sodium salicylate by dialysis method (Liebmann et al., 1994). In brief, 1 ml of NP/PTX solution (containing 0.1 mg PTX) was introduced into a dialysis bag (MWCO = 3,500 Da, Greenbird Inc., Shanghai, China) and the endsealed dialysis bag was submerged fully into 80 ml of 1 M sodium salicylate solution at 37 °C with stirring at 120 rpm for 48 h. At appropriate time intervals (0, 15 and 30 min and 1, 2, 4, 6, 8, 10, 12, 24 and 48 h), 1 ml aliquots were withdrawn and replaced with an equal volume of fresh medium. 2 ml of dichloromethane (DCM) was used to extract the released PTX, and after the DCM was evaporated, the pellet was reconstituted in 1 ml of acetonitrile/water (60:40, v/v) for HPLC measurement. PTX released from stock solution and Taxol injection were also conducted under the same condition as controls. The concentration of PTX in samples was determined by HPLC as described above with correction for the volume replacement.

2.5. Physical status of PTX in the NP

The physical state of PTX loaded in the NP freeze dried and the pristine PTX was investigated by DSC (DSC 204, NETZSCH, Germany) under nitrogen atmosphere at flow rate of 20 ml/min. 10 mg NP/PTX was heated from 20 to 280 °C at speed of 10 °C/min. Indium was used as the standard reference material to calibrate the temperature and energy scales of the DSC instrument (Hu et al., 2007).

2.6. In vitro cellular uptake of nanoparticles

Fluorescent nanoparticles were prepared by incorporating coumarin 6 instead of PTX in the formulations as described in Section 2.2. Twelve-well plates were seeded with 10^5 U87MG cells per well and the cells were incubated at 37 °C for 24 h to allow cell attachment. After 24 h, the medium was replaced by coumarin 6-labled NP for 30 min, 1 h and 2 h. After incubation, the nanoparticles were removed and the wells were washed with ice-cold PBS and then visualized under fluorescent microscope (Leica DMI 4000B, Germany).

2.7. In vitro cytotoxicity assay

U87MG cells in the logarithmic growth phase were seeded at 8,000 cells/well in DMEM supplemented with 10% (v/v) fetal calf serum, 100 U/ml penicillin and 100 μg/ml streptomycin in 96-well plates, and cultured at 37 °C with 5% CO_2 under fully humidified conditions. After 24 h of incubation, cells were treated with 200 μl medium containing either respective drug samples—free drug dissolved in DMSO, NP/PTX and Taxol injection with various concentration or excipient—the blank MPEG–PTMC NP and Cremophor EL with concentration ranging from 0.1 to 1000 μg/ml. After 72 h incubation, MTT was added to the medium to a final concentration of 0.5 mg/ml and the cells were then put back to the incubator for another 4 h. Afterwards, 200 μl of DMSO was added to each well to dissolve any purple formazan crystals formed. The plates were vigorously shaken before measuring the relative color intensity. The absorbance at 570 nm of each well was measured by a microplate reader (Tecan Safire 2, Switzerland).

2.8. In vivo pharmacokinetic study

Fifteen male Sprague–Dawley (SD) rats weighting 200 ± 20 g were randomly assigned to three groups for pharmacokinetic investigation. Group 1 and 2 received an i.v. injection of Taxol or NP/PTX through the tail vein, respectively, at an equivalent dose of 5 mg/kg PTX vs the body weight. At time points of 0 (pre-dose), 5, 15 and 30 min, 1, 2, 4, 8, 12 and 24 h post injection, blood samples (0.5 ml) were collected from the orbital vein and centrifuged at 1000 × *g* for 10 min to obtain plasma. The plasma was stored at −70 °C prior to analysis by HPLC. Liquid–liquid extraction was performed prior to analysis. Briefly, 200 μl samples of plasma were mixed with 3 ml of diethyl ether containing 50 μl of 1.0 μg/ml diazepam as an internal standard. The samples were extracted on vortex-mixer for 2 min and then centrifuged at 6000 × *g* for 10 min. Next, the organic layer was transferred to a clean tube and evaporated under a gentle stream of nitrogen. The extraction residue was reconstituted in 100 μl acetonitrile and centrifuged at 1500 × *g* for 5 min before HPLC analysis. The pharmacokinetic parameters were calculated using the DAS (Drug and Statistic for Windows) software (version 2.0).

2.9. Tissue distribution of MPEG–PTMC NP

Non-invasive and real-time NIR imaging systems was used to monitor the biodistribution of MPEG–PTMC NP. The intracranial U87MG glioblastoma model was established by inoculation of 4×10^5 cells (in 5 μl PBS) into the right striatum (1.8 mm lateral, 0.6 mm anterior to the bregma and 3 mm of depth) of male Balb/c nude mice by using a stereotactic fixation device with mouse adaptor. Brain tumor-bearing mice were intravenously injected with 100 μl DiR-labeled MPEG–PTMC NP (DiR encapsulation content 0.2%) 14 days after inoculation, while control group was injected with physiological saline. At pre-determined time points, the mice were sacrificed and their major organs and blood were harvested. Each organ was rinsed with PBS three times and put into the board. Fluorescent images were captured using the Maestro™ in vivo imaging system (CRI, Inc., Woburn, MA; excitation: 700–950 nm, emission: 780 nm long-pass). The Maestro™ optical system consists of an optical head that includes a liquid crystal tunable filter (LCTF, with a bandwidth of 20 nm and a scanning wavelength range of 500–950 nm) with a custom designed, spectrally optimized lens system that relays the image to a scientific-grade megapixel CCD. The tunable filter was automatically stepped in 10 nm increments from 700 to 950 nm while the camera captured images at each wavelength with constant 1 s exposure. The resulting images (spectral cube, containing a spectrum at every pixel) were loaded into Maestro™ 2.10 software and analyzed.

The tissue distribution of MPEG–PTMC NP was quantified by measuring the ratio of NIR fluorescence intensity recorded as total photons per centimeter squared per steradian per dissected organs.

2.10. Intracranial tumor accumulation of MPEG–PTMC NP in vivo

In vivo real-time fluorescence imaging analysis was used to evaluate the effect of tumor accumulation of MPEG–PTMC NP. The

intracranial U87MG glioblastoma model was established as foregoing, and the control mice were treated similarly with PBS only (without U87MG cells). The intracranial U87MG tumor-bearing mice and the control mice were, respectively, injected with Dir-labeled NP via tail vein 12 days after inoculation. The mice were anesthetized and placed on an animal plate heated to 37 °C. The fluorescent scans were performed at various time points (1, 6, 12, 24 and 48 h) post i.v. using the CRI *In Vivo* Multispectral Imaging system.

2.11. In vivo anti-glioblastoma evaluation

The survival times of brain tumor-bearing mice were investigated using Balb/c nude mice of 20 ± 2 g body weight. The intracranial U87MG glioblastoma model was established as described above. The mice were randomly divided into four groups and treated with 100 μl of physiological saline, blank NP, Taxol and NP/PTX (all of 10 mg/kg PTX to body weight) days 8, 10 and 12 post-inoculation. The body weight was monitored and the survival times were recorded.

3. Results and discussion

3.1. Particle size, size distribution, morphology and zeta potential

The mean diameter of NP was about 49 nm with narrow distribution (PDI between 0.10 and 0.18) (Fig. 1A and Table 1). Loading NP with PTX did not visibly affect particle size and size distribution. The zeta potential value of empty NP in 0.001 M NaCl solution (pH 7.4) was −4.06 ± 1.4 mV. The zeta potential of the NP/PTX was slightly lower than that of blank NP. Morphology of polymer NP/PTX was observed by TEM and the image showed that NP/PTX were regularly spherical in shape. The dehydration and shrinkage of the NP during the process for TEM observation might lead to the smaller diameter compared with the results from DLS. In the TEM photos, "PEG corona" on the NP surface could be observed (Fig. 1B).

3.2. Drug encapsulation efficiency and drug loading content

With increasing PTX feeding ratio, the encapsulation efficiency decreased, however, the drug-loading content first increased and then decreased. Therefore, maximum encapsulation efficiency was in group with minimum drug-loading content. Fortunately, the drug-loading content could reach 6.17 ± 0.44% along with 94.3 ± 4.3% encapsulation efficiency when the PTX feeding ratio was 6.54%.

3.3. In vitro drug release behavior of NP/PTX

Prior to conducting the release assays, PTX release from stock solution and Taxol injection were assessed as controls. It was found that >95% PTX in the stock solution and nearly 87% of PTX in Taxol injection were released within the first 3 h. This suggested that PTX could freely diffuse through the dialysis membrane. As observed in Fig. 1C, the release behavior of PTX from NP/PTX exhibited a biphasic pattern characterized by a fast initial release during the first 3 h, followed by a slower and continuous release. This result showed that NP carriers could not only solubilize the poorly soluble drugs, but also sustain PTX release. In comparison to the reported data

Table 1
Particles size and zeta potential of the nanoparticles ($n = 3$).

Nanoparticles	Size (nm)	Polydisperity	Zeta potentional (mv)
Blank NP	49.3 ± 2.8	0.11 ± 0.03	−4.06 ± 1.4
NP/PTX	49.5 ± 3.1	0.15 ± 0.06	−3.68 ± 1.1

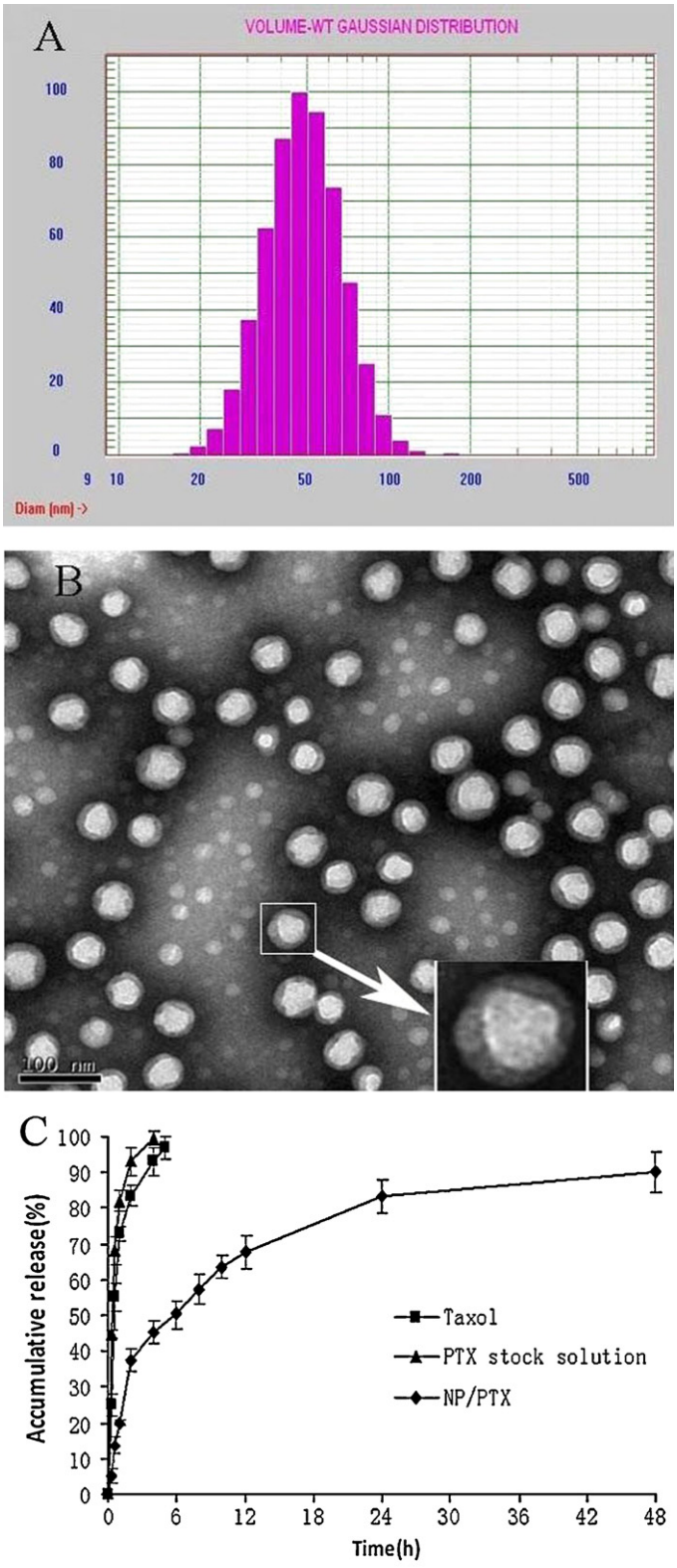

Fig. 1. Particle size and size distribution of PTX-loaded MPEG–PTMC nanoparticles by DLS (A); TEM image of PTX-loaded MPEG–PTMC nanoparticles, the bar is 100 nm (B); release profiles of PTX from of MPEG–PTMC nanoparticles in 1 M sodium salicylate medium at 37 °C. Each point represents the mean ± standard deviation ($n = 3$).

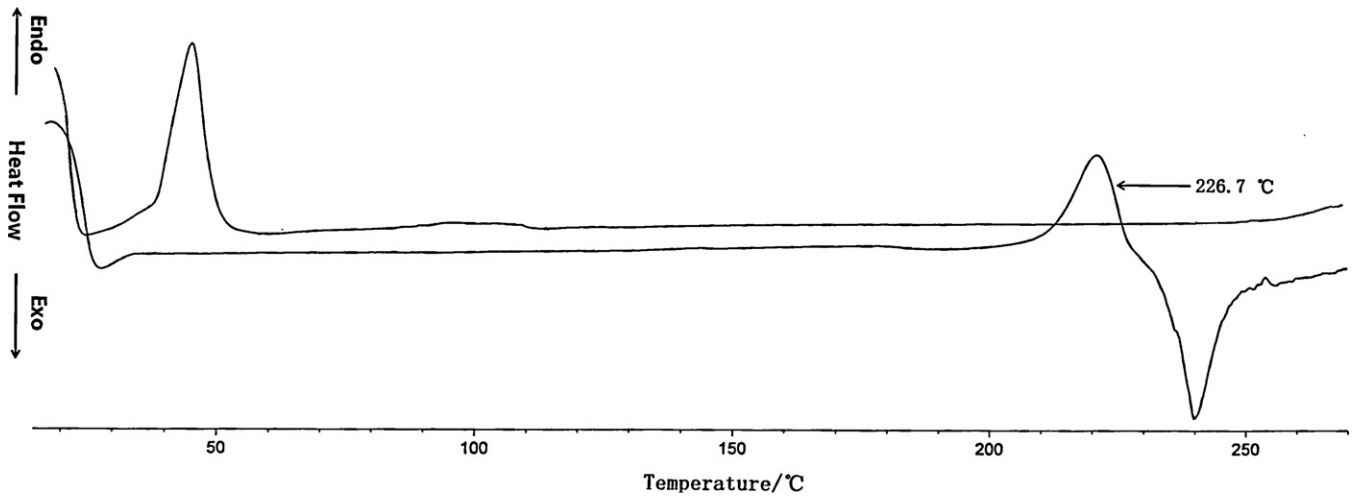

Fig. 2. Differential scanning calorimetry (DSC) thermograms of PTX and PTX-loaded PEG-PTMC nanoparticles.

on similar systems, our nanoparticles loaded PTX exhibited much faster release rate than the nanoparticles encapsulated dexamethasone reported by Zhang et al. (2006a), and possible reasons of the discrepancy might be the different copolymer molecular weight and nanoparticles preparation method, and the distinct diffusion features of PTX and dexamethasone from nanoparticles. Moreover, the presence of high percentage of PEG segment in copolymer matrix, which reduced the hydrophobic interactions of the copolymer and PTX, induced easier soakage and penetration of water into nanoparticles. All these factors could accelerate the release of PTX from nanoparticles.

3.4. Physical status of PTX in the NP

DSC thermograms of the PTX and the PTX-loaded nanoparticles were shown in Fig. 3, from which we can see that an endothermic melting peak was exhibited at 226.7 °C for the pristine PTX (Fig. 2). This peak disappeared for the PTX-loaded nanoparticles, indicating that PTX formulated in the nanoparticles existed as an amorphous state or a solid solution in the polymer matrix.

3.5. Uptake characteristic of nanoparticles by U87MG cells in vitro

Coumarin 6-labeled nanoparticles (the in vitro release kinetics of coumarin 6-loaded NP (drug-loading content 0.04%) indicated that less than 0.5% of coumarin 6 released from the NP within 48 h, data are shown in the online version of this article as Supplementary Materials were used to investigate cellular uptake characteristic, the results of which were shown qualitatively using fluorescent images. U87 MG cells treated with coumarin 6-labeled NP exhibited fluorescent intensity corresponding to incubation

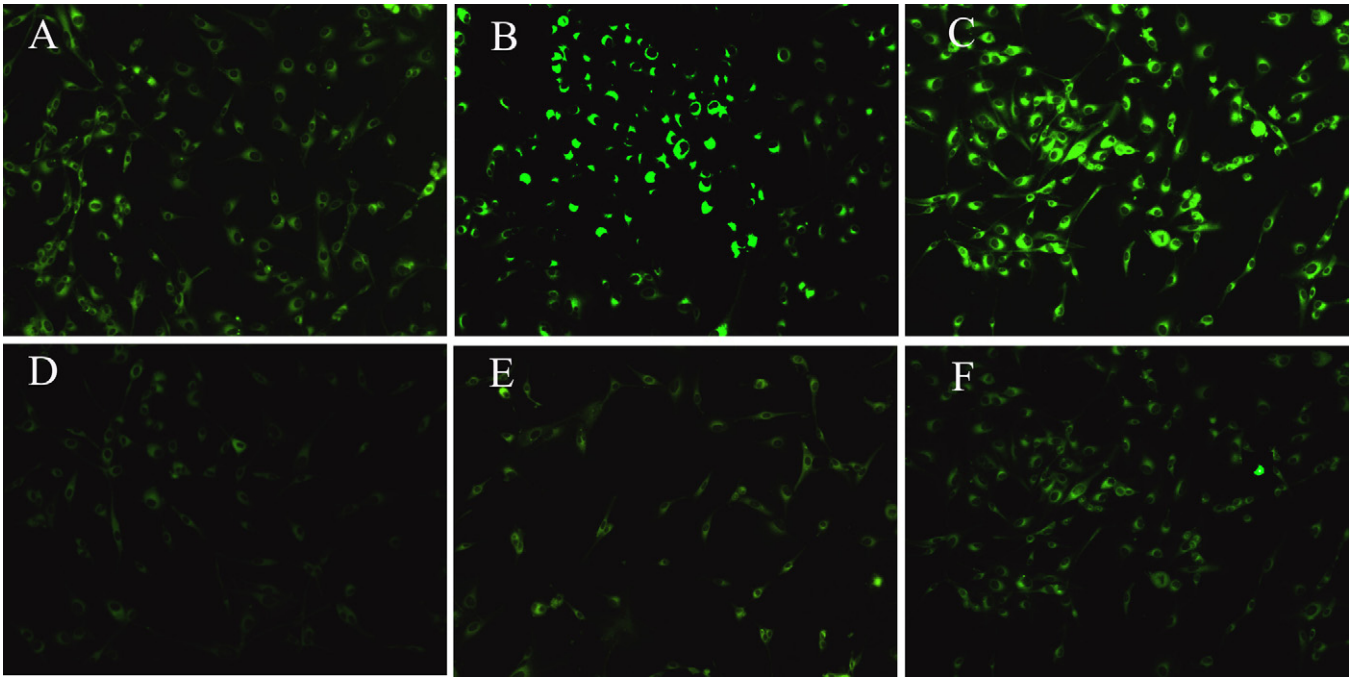

Fig. 3. Cell uptake of coumarin 6-labeled NP after incubating at 37 °C for 30 min (A), 60 min (B) and 120 min (C) and at 4 °C for 30 min (D), 60 min (E) and 120 min (F) was examined by fluorescent microscopy. Concentration of nanoparticles of all samples was adjusted to 300 μg/ml. Green: coumarin-labeled NP. Original magnification: 20×. (For interpretation of the references to color in this figure legend, the reader is referred to the web version of the article.)

time (Fig. 3A–C). The cellular uptake of coumarin 6-labeled NP exhibited a time-dependent mode. In addition, cellular uptake of coumarin 6-labeled NP at 4 °C (Fig. 3E-F) was inhibited compared with that at 37 °C. Therefore, the cellular uptake of NP was also energy-dependent.

3.6. Cytotoxicity assay

In the concentration ranges (0.1–1000 μg/ml) of blank MPEG–PTMC NP, no cytotoxicity was observed (Fig. 4A). However, at the concentration of 1 mg/ml, Cremophor EL displayed significant cytotoxicity, which was well consistent with previous reports (Xin et al., 2010; Liebmann et al., 1994), and this effect might be partly due to the cytostatic action of Cremophor EL. In addition, at the identical concentration, Cremophor EL also exhibited much higher cytotoxicity than MPEG–PTMC copolymer.

The in vitro cytotoxicity of NP/PTX was also investigated, compared with that of the free drug and Taxol injection. After incubation for 72 h, the IC_{50} values were 0.069 μg/ml for free PTX, 0.058 μg/ml for Taxol and 0.051 μg/ml for NP/PTX, respectively (Fig. 4B). Compared with free drug and Taxol injection, NP/PTX displayed similar cytotoxicity. However, it should be noticed that in the case of Taxol significant effect could be attributed to the excipient Cremophor EL. And thus, PTX-entrapped polymer NP represented slightly higher activity than those of free PTX and Taxol in inhibiting the growth of U87MG cells.

3.7. In vivo pharmacokinetic study

The blood clearance curves for paclitaxel loaded in NP after intravenous administration to SD rats are shown in Fig. 5. The NP/PTX showed initial high blood circulating levels compared to Taxol, while paclitaxel formulated in Taxol was quickly removed from the circulating system at 6 h after administration. On the contrary, NP/PTX exhibited a markedly delayed blood clearance. Compartmental analysis of the plasma concentrations showed a significant change in pharmacokinetic parameters of PTX in NP compared to that of commercial formulation (Table 2). It was shown that NP/PTX could extend the elimination half-life ($t_{1/2\beta}$) of Taxol from 4.19 h to 12.19 h ($P < 0.01$). Meanwhile, the area under the paclitaxel plasma concentration-time curve ($AUC_{0\to\infty}$) increased by about 7.17-fold for NP/PTX compared to Taxol. In addition, MRT for the formulations of NP/PTX was 5.85-fold higher

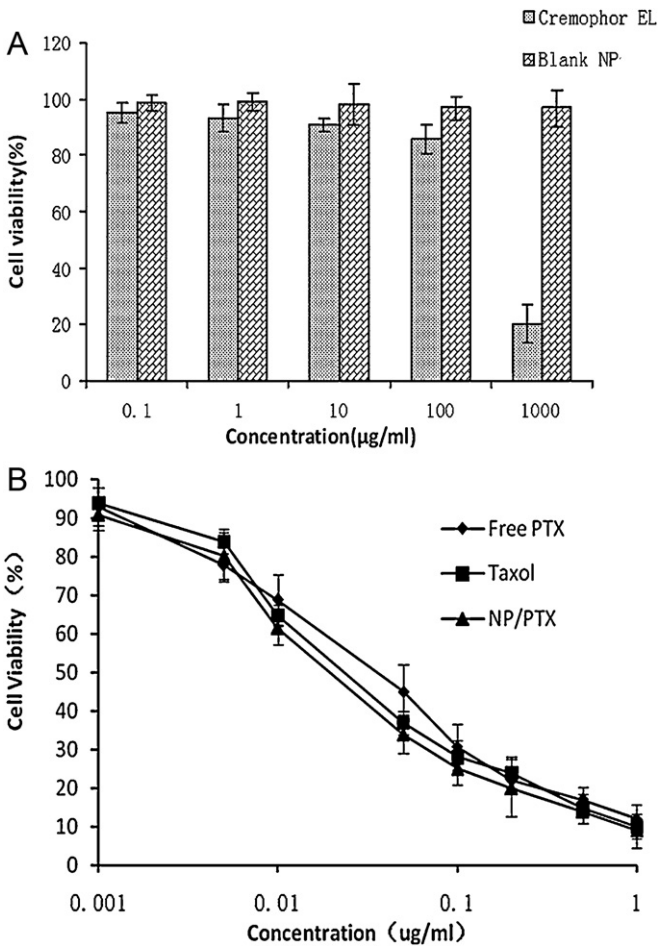

Fig. 4. Viability of U87MG cells as a function of varying concentrations of excipients (MPEG–PTMC and Cremophor EL) (A); in vitro cytotoxicity of different formulations of PTX against U87MG cells (B). Each point represents the mean ± standard deviation ($n = 3$).

than Taxol ($P < 0.01$). In contrast, CL for NP/PTX was significantly lower than that of Taxol implying a longer retention of the drug in blood circulation. Although Taxol can alter the biodistribution of PTX as a result of entrapment of the drug into the circulating

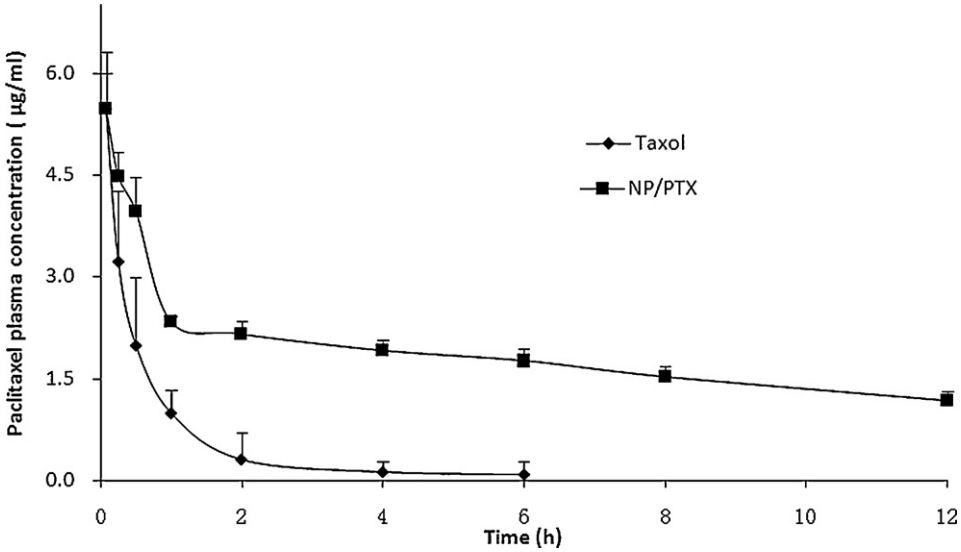

Fig. 5. Plasma concentration–time curves of Taxol and NP/PTX after i.v. administration to SD rats at the same 5 mg/kg PTX dose ($n = 5$).

Table 2
Comparative pharmacokinetic parameters of PTX formulations.

Parameters	Formulations	
	Taxol	NP/PTX
$t_{1/2(\alpha)}$ (h)	0.31	0.28
$t_{1/2(\beta)}$ (h)	4.19	12.29**
$AUC_{0\to t}$ (μg/(L h))	4608.46	21797.13**
$AUC_{0\to\infty}$ (μg/(L h))	6014.49	43140.96**
MRT (h)	2.97	17.38**
CL (L/(h kg))	0.83	0.12*
V_d (L/kg)	0.87	0.82

* $P < 0.05$, compared with Taxol.
** $P < 0.01$, compared with Taxol.

Cremophor EL micelles (Gelderblom et al., 2001; Sparreboom et al., 1999), the pharmacokinetic results indicated that the PEG–PTMC NP had much longer systemic circulation time and much slower plasma elimination rate than those of Taxol. This long blood circulation could be illustrated by the stealth behavior of polymer nanoparticles induced by hydrophilic shell of PEG, which will reduce the absorption by plasma proteins and decrease the rate of mononuclear phagocyte system (MPS) uptake. Therefore, these results illustrated the potential utility of PEG–PTMC nanoparticles as long circulating reservoir for hydrophobic anticancer agents.

3.8. Tissue distribution of MPEG–PTMC NP

Non-invasive and real-time NIR imaging systems could be used to monitor the fate of drug-loaded nanocarriers in vivo, and aid in the identification of key factors influencing biodistribution, pharmacokinetics and tumor accumulation of various drug carriers (Park et al., 2007). At 1 h post-injection, strong fluorescence intensities were observed in the liver and spleen, indicating a large number of MPEG–PTMC NP subjected to uptake by RES (Fig. 6B). Fortunately, after 12 h post-injection, NIR fluorescence intensity in intracranial tumor tissue was increased, whereas that in blood and other organs, such as liver, spleen, lung and heart, was gradually decreased. On the basis of organ imaging, mean fluorescence intensities of heart, liver, spleen, lung, kidney, blood, and the illuminated region of brains were calculated. Fig. 6C displays the detailed quantitative results on tissue distribution and brain tumor regions accumulation as a function of time. The fluorescence intensity in the heart, liver, spleen, lung, and blood decreased similarly. The NIR fluorescence intensities of MPEG–PTMC NP in brain tumor regions reached a peak at 12 h post-injection, maintained about 12 h, and then decreased gradually. The significant tumor targeting of MPEG–PTMC NP may be interpreted by the long-term blood circulation time. DiR-labled NP could even be detected in the blood at 48 h post i.v., implying that drug-loaded nanoparticles were relatively stable in the bloodstream. Indeed, brain tumors have a compromised endothelial barrier which facilitates molecular transport. Long-circulating nanoparticles were found either to accumulate at the margins of the brain tumor (Enochs et al., 1999; Grabb and Gilbert, 1995) or to be taken up by the tumor cells and macrophages in tumor. Additionally, the in vitro release kinetics of DiR-loaded NP (drug-loading content 0.2%) was investigated by dialysis method. It indicated that only less than 1% of DiR released from the NP within 72 h (data not shown). Therefore, it was DiR-labeled NP penetrated into tumor and major organs but not free DiR in the real-time NIR imaging analysis.

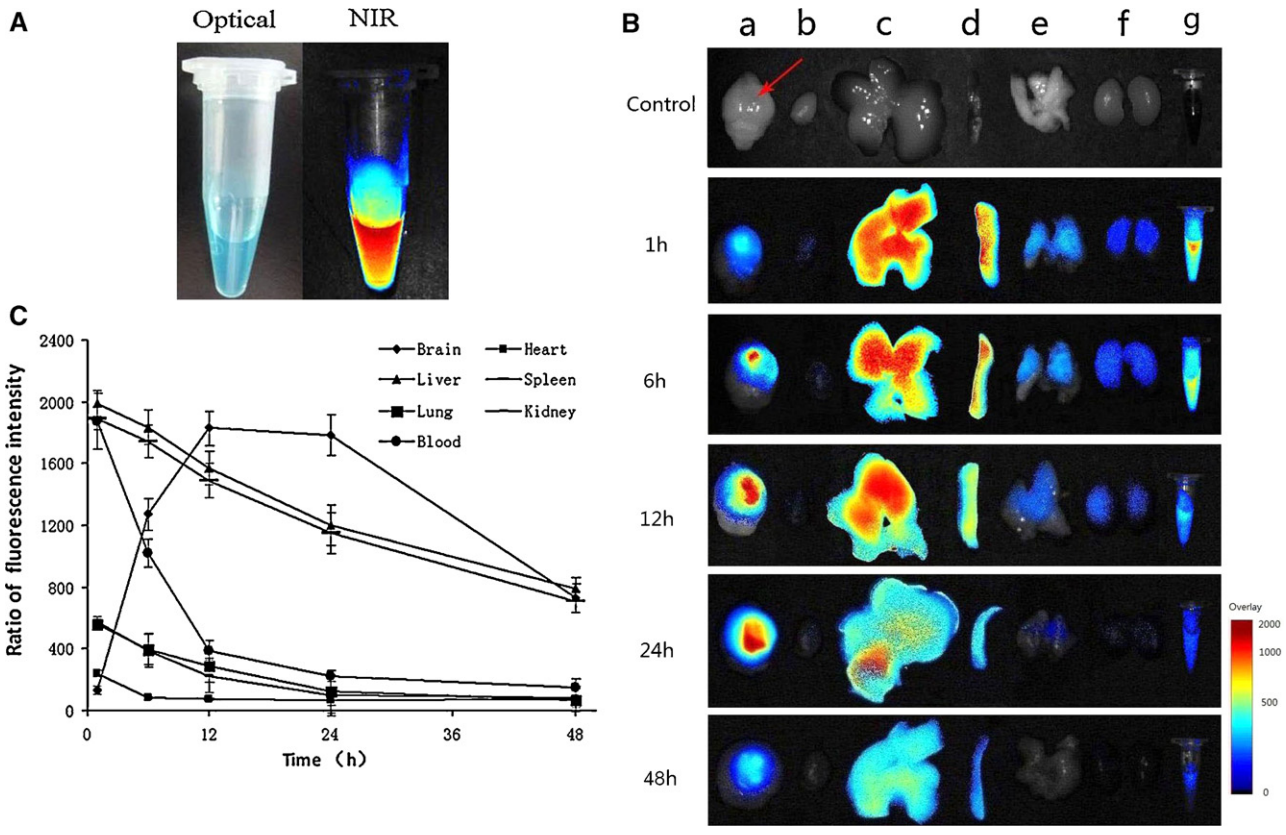

Fig. 6. White light and NIR fluorescence images of DiR-labeled NP (A); representative ex vivo NIR fluorescence images of dissected organs of mice bearing U87MG glioma sacrificed at 1, 6, 12, 24 and 48 h after intravenous injection of DiR-labeled NP: a, brain; b, heart; c, liver; d, spleen; e, lung; f, kidney; g, blood. The tumor location is specified with a red arrow (B); ratio of the relative fluorescence intensity in dissected organs as a function of time after intravenous injection of DiR-labeled NP (C). Data are presented as means ± standard deviation ($n = 3$). (For interpretation of the references to color in this figure legend, the reader is referred to the web version of the article.)

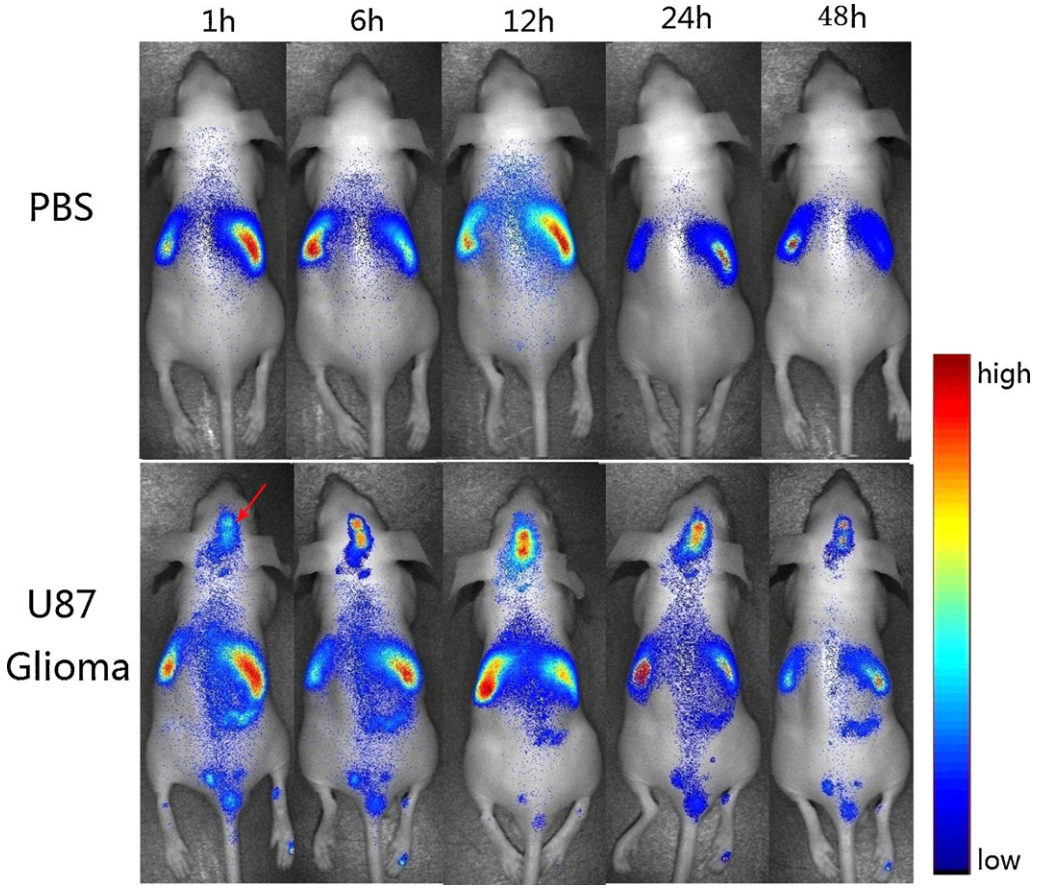

Fig. 7. In vivo NIR fluorescence images of brain tumor-bearing mice and control mice after intravenous injection of DiR-labeled NP. The tumor location is specified with a red arrow. (For interpretation of the references to color in this figure legend, the reader is referred to the web version of the article.)

3.9. Intracranial tumor accumulation of MPEG–PTMC NP in vivo

As shown in Fig. 7, at all of the survey points, little fluorescence signal was detected in the brains of control mice. However, in intracranial tumor regions of glioblastoma-bearing mice, MPEG–PTMC NP revealed significant tumor accumulation. The fluorescence intensity exhibited time-dependent changes, and displayed a maximum fluorescence signal at 12 h post i.v. The mechanism by which NP penetrated across BBB has so far not been totally explained. In our study, the results indicated that blood–brain barrier (BBB) was partly impaired by tumor growth in xenograft glioblastoma model (the inoculation method did not disrupt BBB), which is consistent with the previous study (Xin et al., 2010; Zhan et al., 2010). And thus, MPEG–PTMC NP could target to high-grade glioma via EPR effect where nanoparticles spontaneously accumulate in the pathological area due to PEG hydrophilic surface and long-term blood circulation.

3.10. In vivo antitumor efficacy

Fig. 8A represents Kaplan–Meier survival curves. After 1 week treatment, the median survival time of mice treated with NP/PTX (27 days) was significantly longer than those of mice treated with physiological saline (21 days, $P<0.001$), Taxol injection (24 days, $P<0.05$) and unloaded NP (21 days, $P<0.001$) through log-rank analysis, respectively (Table 3). The result might be explained by the increased local concentration of PTX in the tumor tissue via EPR effect, prolonged blood circulation time and sustained release profiles. Another reason could be that BBB was destructed to some extent upon tumor growth, even though it is still controversial (de Vries et al., 2009; Fomchenko and Holland, 2006). The change in body weight was also recorded in 11 days post i.v. because the mice in physiological saline group died on day 19 after implantation. At the identical days there was much less body weight loss in mice of NP/PTX group than that of mice in any other three groups (Fig. 8B). Compared to physiological saline group, blank NP group mice exhibited similar median survival time and weight loss during the experimental period, indicating that MPEG–PTMC nanoparticles were safe carriers. Taken together, NP/PTX developed in our study could not only induce less systemic toxicity, but also increase anti-tumor efficacy.

Table 3
Median survival time for glioma implanted mice of different therapeutic groups.

Group	Dose (mg/kg)	Median (day)	Log-rank test		
			vs saline	vs blank NP	vs Taxol
Saline	–	21	–	–	–
Blank NP	153	21	$P>0.05$	–	–
Taxol	10	24	*	*	–
NP/PTX	10	30	**	**	*

* $P<0.05$.
** $P<0.01$.

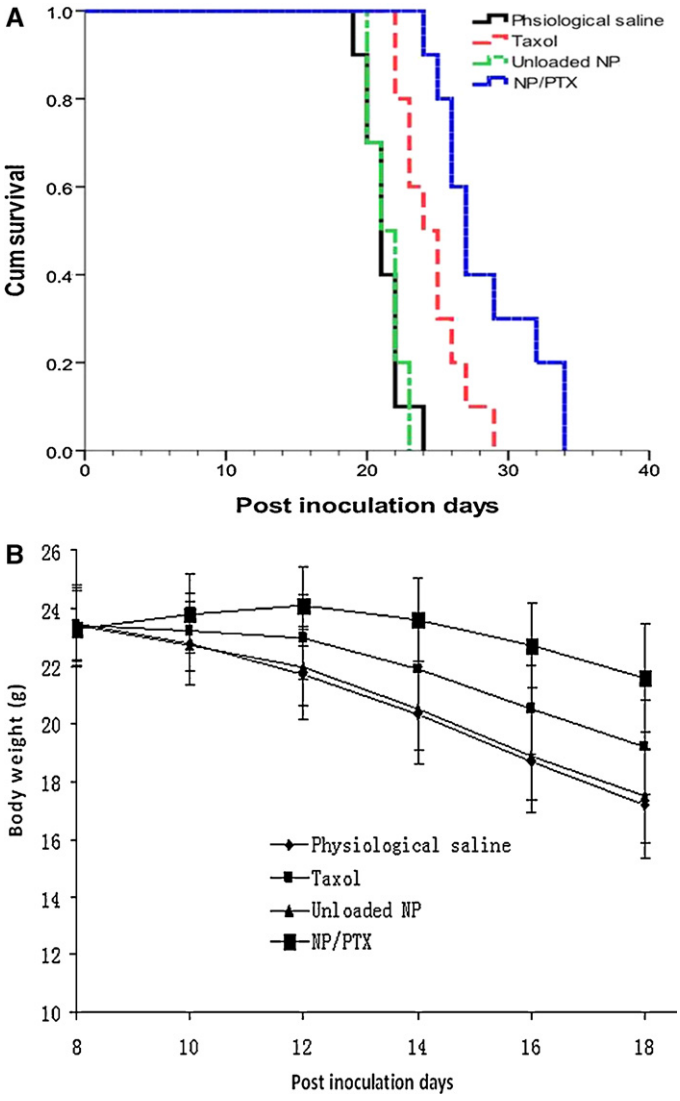

Fig. 8. Kaplan–Meier survival curves of intracranial U87MG glioblastoma-bearing mice treated with NP/PTX and Taxol at days 8, 10 and 12 (1 week treatment) after inoculation (each dosing 10 mg/kg PTX). Arrows indicate the time of therapeutic injections (A); changes in body weight of mice as a function of time in intracranial U87MG glioma-bearing mice (B) ($n = 8$).

4. Conclusions

In this study, biodegradable nanoparticles were prepared from amphiphilic MPEG–PTMC diblock copolymer by the emulsion/solvent evaporation technique for controlled release of an antineoplastic drug (PTX). The optimized formulation with ideal drug-loading content and encapsulation efficiency had the particle size around 49 nm. In vitro, PTX-loaded nanoparticles displayed sustained release and noticeable anti-tumor efficacy slightly higher than Taxol injection. The pharmacokinetic and biodistribution studies demonstrated that NP/PTX could significantly increase the blood circulation time of PTX. In vivo real-time image also exhibited significant brain tumor passive targeting. In addition, the therapeutic improvement of PTX-loaded nanoparticles in vivo against intracranial U87MG glioblastoma was also obtained based on the effect of passive tumor targeting. Taken together, MPEG–PTMC nanoparticles developed in this study may be a potential delivery system for improving the limited penetration of PTX in advanced GMB.

Acknowledgements

The work was supported from the National Basic Research Program of China 973 program (2007CB935802), National Natural Science Foundation of China (30873177) and National Science and Technology Major Project (2009ZX09310-006).

Appendix A. Supplementary data

Supplementary data associated with this article can be found, in the online version, at doi:10.1016/j.ijpharm.2011.08.052.

References

Danhier, F., Lecouturier, N., Vroman, B., Jérôme, C., Marchand-Brynaert, J., Feron, O., Préat, V., 2009. Paclitaxel-loaded PEGylated PLGA-based nanoparticles: in vitro and in vivo evaluation. Journal of Controlled Release 133, 11–17.

de Vries, N.A., Beijnen, J.H., van Tellingen, O., 2009. High-grade glioma mouse models and their applicability for preclinical testing. Cancer Treatment Reviews 35, 714–723.

Enochs, W.S., Harsh, G., Hochberg, F., Weissleder, R., 1999. Improved delineation of human brain tumors on MR images using a long-circulating, superparamagnetic iron oxide agent. Journal of Magnetic Resonance Imaging 9, 228–232.

Fomchenko, E.I., Holland, E.C., 2006. Mouse models of brain tumors and their applications in preclinical trials. Clinical Cancer Research 12, 5288.

Gelderblom, H., Verweij, J., Nooter, K., Sparreboom, A., 2001. Cremophor EL: the drawbacks and advantages of vehicle selection for drug formulation. European Journal of Cancer 37, 1590–1598.

Grabb, P.A, Gilbert, M.R., 1995. Neoplastic and pharmacological influence on the permeability of an in vitro blood–brain barrier. Journal of Neurosurgery 82, 1053–1058.

Groothuis, D.R., Vriesendorp, F.J., Kupfer, B., Warnke, P.C., Lapin, G.D., Kuruvilla, A., Vick, N.A., Mikhael, M.A., Patlak, C.S., 1991. Quantitative measurements of capillary transport in human brain tumors by computed tomography. Annals of Neurology 30, 581–588.

Han, J., Chen, T.X., Branford-White, C.J., Zhu, L.M., 2009. Electrospun shikonin-loaded PCL/PTMC composite fiber mats with potential biomedical applications. International Journal of Pharmaceutics 382, 215–221.

Hu, Y., Xie, J., Tong, Y.W., Wang, C.H., 2007. Effect of PEG conformation and particle size on the cellular uptake efficiency of nanoparticles with the HepG2 cells. Journal of Controlled Release 118, 7–17.

Huang, S., Li, J., Han, L., Liu, S., Ma, H., Huang, R., Jiang, C., 2011. Dual targeting effect of Angiopep-2-modified. DNA-loaded nanoparticles for glioma. Biomaterials.

Kleihues, P., Burger, P.C., Scheithauer, B.W., 1993. The new WHO classification of brain tumours. Brain Pathology 3, 255–268.

Law, M., Yang, S., Babb, J.S., Knopp, E.A., Golfinos, J.G., Zagzag, D., Johnson, G., 2004. Comparison of cerebral blood volume and vascular permeability from dynamic susceptibility contrast-enhanced perfusion MR imaging with glioma grade. American Journal of Neuroradiology 25, 746.

Leggett, D.A.C., Miles, K.A., Kelley, B.B., 1998. Blood–brain barrier and blood volume imaging of cerebral glioma using functional CT: a pictorial review. Australasian Radiology 42, 335–340.

Liebmann, J., Cook, J.A., Lipschultz, C., Teague, D., Fisher, J., Mitchell, J.B., 1994. The influence of Cremophor EL on the cell cycle effects of paclitaxel (Taxol®) in human tumor cell lines. Cancer Chemotherapy and Pharmacology 33, 331–339.

Louis, D.N., Ohgaki, H., Wiestler, O.D., Cavenee, W.K., Burger, P.C., Jouvet, A., Scheithauer, B.W., Kleihues, P., 2007. The 2007 WHO classification of tumours of the central nervous system. Acta Neuropathologica 114, 97–109.

Lu, H., Pollack, E., Young, R., Babb, J., Johnson, G., Zagzag, D., Carson, R., Jensen, J., Helpern, J., Law, M., 2008. Predicting grade of cerebral glioma using vascular-space occupancy MR imaging. American Journal of Neuroradiology 29, 373.

Lupo, J.M., Cha, S., Chang, S.M., Nelson, S.J., 2005. Dynamic susceptibility-weighted perfusion imaging of high-grade gliomas: characterization of spatial heterogeneity. American Journal of Neuroradiology 26, 1446.

Mao, S., Shuai, X., Unger, F., Wittmar, M., Xie, X., Kissel, T., 2005. Synthesis, characterization and cytotoxicity of poly(ethylene glycol)-graft-trimethyl chitosan block copolymers. Biomaterials 26, 6343–6356.

Musacchio, T., Laquintana, V., Latrofa, A., Trapani, G., Torchilin, V.P., 2008. PEG-PE micelles loaded with paclitaxel and surface-modified by a PBR-ligand: synergistic anticancer effect. Molecular Pharmaceutics 6, 468–479.

Nikanjam, M., Gibbs, A.R., Hunt, C.A., Budinger, T.F., Forte, T.M., 2007. Synthetic nano-LDL with paclitaxel oleate as a targeted drug delivery vehicle for glioblastoma multiforme. Journal of Controlled Release 124, 163–171.

Park, K., Kim, J.H., Nam, Y.S., Lee, S., Nam, H.Y., Kim, K., Park, J.H., Kim, I.S., Choi, K., Kim, S.Y., 2007. Effect of polymer molecular weight on the tumor targeting characteristics of self-assembled glycol chitosan nanoparticles. Journal of Controlled Release 122, 305–314.

Pego, A., Van Luyn, M., Brouwer, L., Van Wachem, P., Poot, A., Grijpma, D., Feijen, J., 2003. In vivo behavior of poly(1,3-trimethylene carbonate) and copolymers of 1,3-trimethylene carbonate with D,L-lactide or -caprolactone: degradation and tissue response. Journal of Biomedical Materials Research Part A 67, 1044–1054.

Plate, K.H., Risau, W., 1995. Angiogenesis in malignant gliomas. Glia 15, 339–347.

Regina, A., Demeule, M., Che, C., Lavallée, I., Poirier, J., Gabathuler, R., Beliveau, R., Castaigne, J., 2008. Antitumour activity of ANG1005, a conjugate between paclitaxel and the new brain delivery vector Angiopep-2. British Journal of Pharmacology 155, 185–197.

Rokicki, G., 2000. Aliphatic cyclic carbonates and spiroorthocarbonates as monomers. Progress in Polymer Science 25, 259–342.

Sameshima, T., Nabeshima, K., Toole, B.P., Yokogami, K., Okada, Y., Goya, T., Koono, M., Wakisaka, S., 2000. Expression of emmprin (CD147), a cell surface inducer of matrix metalloproteinases, in normal human brain and gliomas. International Journal of Cancer 88, 21–27.

Schneider, S.W., Ludwig, T., Tatenhorst, L., Braune, S., Oberleithner, H., Senner, V., Paulus, W., 2004. Glioblastoma cells release factors that disrupt blood–brain barrier features. Acta Neuropathologica 107, 272–276.

Sparreboom, A., van Zuylen, L., Brouwer, E., Loos, W.J., de Bruijn, P., Gelderblom, H., Pillay, M., Nooter, K., Stoter, G., Verweij, J., 1999. Cremophor EL-mediated alteration of paclitaxel distribution in human blood. Cancer Research 59, 1454.

Veronese, F.M., 2001. Peptide and protein PEGylation: a review of problems and solutions. Biomaterials 22, 405–417.

Watanabe, J., Kotera, H., Akashi, M., 2007. Reflexive interfaces of poly(trimethylene carbonate)-based polymers: enzymatic degradation and selective adsorption. Macromolecules 40, 8731–8736.

Wolburg, H., Wolburg-Buchholz, K., Kraus, J., Rascher-Eggstein, G., Liebner, S., Hamm, S., Duffner, F., Grote, E.H., Risau, W., Engelhardt, B., 2003. Localization of claudin-3 in tight junctions of the blood–brain barrier is selectively lost during experimental autoimmune encephalomyelitis and human glioblastoma multiforme. Acta Neuropathologica 105, 586–592.

Xin, H., Chen, L., Gu, J., Ren, X., 2010. Enhanced anti-glioblastoma efficacy by PTX-loaded PEGylated poly(-caprolactone) nanoparticles: in vitro and in vivo evaluation. International Journal of Pharmaceutics 402, 238–247.

Zhan, C., Gu, B., Xie, C., Li, J., Liu, Y., Lu, W., 2010. Cyclic RGD conjugated poly(ethylene glycol)-co-poly(lactic acid) micelle enhances paclitaxel anti-glioblastoma effect. Journal of Controlled Release 143, 136–142.

Zhang, Y., Zhang, Q., Zha, L., Yang, W., Wang, C., Jiang, X., Fu, S., 2004. Preparation, characterization and application of pyrene-loaded methoxy poly(ethylene glycol)–poly(lactic acid) copolymer nanoparticles. Colloid and Polymer Science 282, 1323–1328.

Zhang, Z., Grijpma, D.W., Feijen, J., 2006a. Poly(trimethylene carbonate) and monomethoxy poly(ethylene glycol)-block-poly(trimethylene carbonate) nanoparticles for the controlled release of dexamethasone. Journal of Controlled Release 111, 263–270.

Zhang, Z., Grijpma, D.W., Feijen, J., 2006b. Thermo-sensitive transition of monomethoxy poly(ethylene glycol)-block-poly(trimethylene carbonate) films to micellar-like nanoparticles. Journal of Controlled Release 112, 57–63.

Zhang, Z., Kuijer, R., Bulstra, S.K., Grijpma, D.W., Feijen, J., 2006c. The in vivo and in vitro degradation behavior of poly(trimethylene carbonate). Biomaterials 27, 1741–1748.

Zhao, H., Wang, J.C., Sun, Q.S., Luo, C.L., Zhang, Q., 2009. RGD-based strategies for improving antitumor activity of paclitaxel-loaded liposomes in nude mice xenografted with human ovarian cancer. Journal of Drug Targeting 17, 10–18.

Zhu, K., Hendren, R., Jensen, K., Pitt, C., 1991. Synthesis, properties, and biodegradation of poly(1,3-trimethylene carbonate). Macromolecules 24, 1736–1740.

Zülch, K., 1980. Principles of the new World Health Organization (WHO) classification of brain tumors. Neuroradiology 19, 59–66.